Strong field ionization rates simulated with time-dependent configuration interaction and an absorbing potential

Pascal Krause, Jason A. Sonk, and H. Bernhard Schlegel

Citation: The Journal of Chemical Physics **140**, 174113 (2014); doi: 10.1063/1.4874156
View online: http://dx.doi.org/10.1063/1.4874156
View Table of Contents: http://scitation.aip.org/content/aip/journal/jcp/140/17?ver=pdfcov
Published by the AIP Publishing

Strong field ionization rates simulated with time-dependent configuration interaction and an absorbing potential

Pascal Krause, Jason A. Sonk, and H. Bernhard Schlegel
Department of Chemistry, Wayne State University, Detroit, Michigan 48202-3489, USA

(Received 24 February 2014; accepted 17 April 2014; published online 7 May 2014)

Ionization rates of molecules have been modeled with time-dependent configuration interaction simulations using atom centered basis sets and a complex absorbing potential. The simulations agree with accurate grid-based calculations for the ionization of hydrogen atom as a function of field strength and for charge resonance enhanced ionization of H_2^+ as the bond is elongated. Unlike grid-based methods, the present approach can be applied to simulate electron dynamics and ionization in multi-electron polyatomic molecules. Calculations on HCl^+ and HCO^+ demonstrate that these systems also show charge resonance enhanced ionization as the bonds are stretched. © *2014 AIP Publishing LLC*. [http://dx.doi.org/10.1063/1.4874156]

I. INTRODUCTION

The advancements in the creation of intense laser pulses with femto-second (fs) and atto-second (as) durations[1,2] have, literally, shed a new light on matter. As these pulse durations have reached the limit in which electron motion takes place, new mechanistic insights are needed. This has brought considerable interest to processes such as above threshold ionization (ATI) and high-order harmonic generation (HHG), for example. Sub-fs laser pulses are now available in the extreme ultraviolet (XUV), permitting real-time observation of electron dynamics in atoms[3,4] on timescales when ionization and electron transfer takes place,[5] as well as enabling the mapping of the shape of individual orbitals.[6]

A theoretical description of electronic and molecular effects induced by strong sub-fs pulses cannot be captured completely by static models, so that explicitly time-dependent methods are needed. The quantum description of the electron dynamics is governed by the time-dependent Schrödinger equation (TDSE) for many-electron wavefunctions. The simulation of correlated electronic motion is a challenging task, even with the computer resources currently available.

For one- and two-electron systems, ionization rates can be obtained from highly accurate 3D simulations of the TDSE using grid-based methods and basis set expansion approaches (for leading references see Refs. 7–12, and references therein; for a recent review, see Ref. 13). For many-electron systems, strong field simulations have been carried out within the framework of time-dependent Hartree-Fock (TDHF)[14] and time-dependent density functional theory (TDDFT),[15] and for correlated wavefunction methods such as time-dependent configuration interaction (TDCI),[16–19] time-dependent coupled cluster (TDCC),[20,21] and multi-configuration time-dependent Hartree-Fock (MCTDHF).[22–25]

While TDDFT can treat many-electron systems approximately, TDCI methods in principal can be improved systematically towards the exact solution. Time-dependent configuration interaction methods have been shown to be a powerful tool for insights in the light-induced dynamics of bound electrons, e.g., response properties[26,27] as well as for state-to-state excitations within a few fs,[28–30] or for the description of charge migration by direct ionization.[31–33]

Electronic structure calculations for molecules are typically carried out with atom-centered basis functions. Standard basis sets can be used to calculate higher harmonic generation, but not up to the cut-off region where ionization takes place.[26] Because atom-centered basis functions cannot describe the continuum, the direct simulation of the ejection of an electron from a bound state is not possible with this approach. Approximate treatments of ionization have been employed for TDDFT[34] and TDCI[35] by introducing complex excitation energies to model loss of electron density. Uhlmann *et al.*[34] assumed that all DFT states above the ionization potential are absorbing. In Klamroth's heuristic model,[35] lifetimes for CI states have been approximated based on orbital energies and an escape distance. With very large basis sets augmented with numerous diffuse shells and off-centered functions, Head-Gordon and co-workers[36] were able to calculate high energy Rydberg states and to compute the HHG spectrum of hydrogen atom using Klamroth's heuristic model to account for ionization.

In the present work, we provide an alternate model for ionization using an absorbing potential in real space. Our simulations of ionization employ the TDCI method using atom-centered basis functions in combination with an absorbing boundary potential. In this paper, we present the calculation of ionization rates for hydrogen atom and hydrogen molecule cation. These one-electron system serve as benchmark systems, where accurate reference calculations are available.[7–11,13] To demonstrate the applicably of our model to multi-electron systems, we calculate the ionization rates of hydrogen chloride cation and formyl cation. For these species we report enhanced ionization during bond dissociation. All formulas and values are given in atomic units, except for the time, which is, for convenience, given in fs.

II. THEORY

A. Time-dependent configuration interaction

The quantum dynamics of the electron density of a molecule in a laser field can be obtained by solving the TDSE for electronic wavefunctions:

$$\mathrm{i}\frac{\partial}{\partial t}\Psi_{\mathrm{el}}(t) = \hat{\mathbf{H}}(t)\Psi_{\mathrm{el}}(t). \tag{1}$$

The total Hamilton operator is time-dependent because of the interaction of the electrons with the external electric field of the light which is given in the semi-classical dipole approximation. An absorbing potential $\hat{\mathbf{V}}^{\mathrm{Absorb}}$ is added to the Hamiltonian to simulate the loss of electron density due to ionization

$$\hat{\mathbf{H}}(t) = \hat{\mathbf{H}}_{\mathrm{el}} - \hat{\vec{\mu}}\vec{E}(t) - \mathrm{i}\hat{\mathbf{V}}^{\mathrm{Absorb}}. \tag{2}$$

The form of the absorbing potential is discussed in more detail in Subsection II B. $\vec{E}(t)$ is the electric field component of the laser and $\hat{\vec{\mu}}$ the dipole operator. The present study uses linearly polarized cosine square shaped pulses

$$\vec{E}(t) = \vec{s}(t)\cos\left[\omega t - \phi\right] \tag{3}$$

$$\vec{s}(t) = \begin{cases} \vec{E}_0 \cos^2\left(\frac{\pi}{2\sigma}t\right) & \text{for } -\sigma < t < \sigma \\ \vec{0} & \text{else,} \end{cases} \tag{4}$$

ϕ is the phase and 2σ is the full duration of the pulse.

The time-dependent wavefunction is expanded in terms of ground and excited states of the field-free, time-independent Hamiltonian, $\hat{\mathbf{H}}_{\mathrm{el}}|\Psi_i\rangle = \omega_i|\Psi_i\rangle$:

$$\Psi(t) = \sum_{i=0} C_i(t)|\Psi_i\rangle. \tag{5}$$

Using this *ansatz*, Eq. (1) reduces to a set of coupled differential equations for the time-dependent coefficients:

$$\mathrm{i}\frac{\partial}{\partial t}C_i(t) = \sum_j H_{ij}(t)C_j(t), \tag{6}$$

where $H_{ij}(t) = \langle\Psi_i|\hat{\mathbf{H}}(t)|\Psi_j\rangle$. The evolution of the coefficients is solved numerically using a unitary transformation at the midpoint of the time step:

$$\vec{C}(t + \Delta t) = \exp[-\mathrm{i}\mathbf{H}(t + \Delta t/2)\Delta t]\vec{C}(t). \tag{7}$$

The exponential of the Hamiltonian matrix is calculated explicitly (rather than with a Trotter or Magnus expansion) with the only approximation being that the electric filed is constant during the time step. Reducing the time step from $\Delta t = 0.05$ $\hbar/\mathrm{E_h}$ to $\Delta t = 0.025$ $\hbar/\mathrm{E_h}$ changed the norm at the end of an intense pulse with a field strength of 0.09 $\mathrm{E_h}/(ea_0)$ by less than 0.02%.

In this work, the field-free wavefunctions of Eq. (5) are obtained from a configuration interaction singles (CIS) calculation[37] using the GAUSSIAN program package.[38] All time-dependent configuration interaction singles (TDCIS) simulations in this work have been carried out using a time step of $\Delta t = 0.05$ $\hbar/\mathrm{E_h}$(1.2 as) and a total propagation time of 1000 $\hbar/\mathrm{E_h}$(24.2 fs), if not stated otherwise.

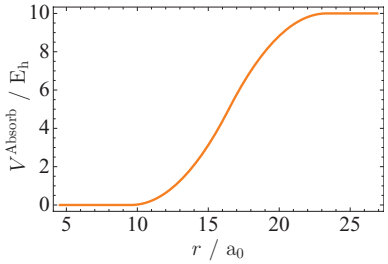

FIG. 1. The radial part of the absorbing potential for hydrogen starting at $r_a = 9.524$ $\mathrm{a_0}$ with piecewise quadratic segments rising to $V_{max} = 10$ $\mathrm{E_h}$.

B. Complex absorbing potential (CAP)

Absorbing potentials are well established for grid based calculations to prevent reflections from the boundaries.[39,40] Examples of absorbing potentials to simulate strong field ionization include the grid based calculations by Hermann and Fleck[7] for hydrogen atom in a static field and studies by Santra and co-workers using TDCIS methods with numerical orbitals for multi-electron atoms.[19] Absorbing potentials have been employed less frequently for polyatomic systems in which basis set expansions are used to represent the wavefunction. For a polyatomic system, the absorbing potential should conform to the shape of the molecule. It needs to be placed far enough from the molecule so that the interaction with the ground state is small and so that the dynamics of the low lying excited states are not strongly perturbed, but close enough so that higher lying excited states interact significantly. The potential should rise smoothly to avoid reflections. The radial component of the absorbing potential for hydrogen atom used in the present work is shown in Fig. 1. The potential has a quadratic rise, starting at r_a, and a quadratic fall-off until V_{max} is reached, with a linear section in between if needed. In the present work, we have chosen r_a equal to 3.5 times the van der Waals radius ($r_a = 9.524$ $\mathrm{a_0}$ for hydrogen), a maximum potential height of $V_{max} = 10$ $\mathrm{E_h}$, and a curvature of 0.21 for the quadratic part.

For molecules, the absorbing potential is constructed from the spherical absorbing potentials around each atom. At a given point, the total absorbing potential is equal to the minimum of the values from the atomic absorbing potentials. The resulting potential resembles the solvent cavity used in polarizable continuum solvation models.[41] The one electron integrals of the absorbing potential are obtained using the numerical integration methods employed in density functional theory (299 radial shells and 974 angular points per shell for each atom).[42,43]

Another criterion which needs attention is the positioning of the CAP. The CAP must be placed outside of the Coulomb well, but within the maximum excursion of an electron in the laser field ($\alpha = E_0/\omega^2 = 18.5$ $\mathrm{a_0}$ for $E_0 = 0.06$ $\mathrm{E_h}/(\mathrm{ea_0})$ and $\omega = 0.057$ $\mathrm{E_h}/\hbar$). The CAP should be placed so that there is still sufficient overlap with the basis functions. The further away the CAP is placed, the more diffuse functions are needed to correctly describe the motion away from the nucleus. However, in order to reduce the numerical effort, the number of diffuse functions needs to be kept relatively small. A

TABLE I. Table of even-tempered exponents for *s*, *p*, *d*, and *f* type Gaussian functions in the medium absorbing basis. The nine exponents marked by asterisk are used in the small absorbing basis set.

s	*p*	*d*	*f*
6.5536	...	...	...
3.2768	...	...	...
1.6384	...	...	...
0.8192	...	...	...
0.4096	0.4096	...	...
0.2048	0.2048	0.2048	...
0.1024	0.1024	0.1024	...
0.0512	0.0512	0.0512*	0.0512
0.0256*	0.0256*	0.0256*	0.0256*
0.0128*	0.0128*	0.0128*	...
0.0064*	...	...	...

compromise has to be found in placing the CAP by carefully testing both basis set and CAP position.

C. The basis sets

To simulate ionization using complex absorbing potentials, the basis set must be include a sufficient number of diffuse functions that interact with the absorbing potential. For hydrogen atom, we started by using a very large basis set: 17 even tempered Gaussian exponents have been generated by the power series: $\alpha_n = \alpha_0 \cdot 2^n$. The exponents of this series range from $\alpha_0 = 0.0001$ to $\alpha_{16} = 6.5536$. For each exponent the angular momentum extends from $l = 0$ to $l = 9$ (from *s* to *l* functions). By systematically deleting basis functions, we were able to obtain a medium-size basis set of even tempered exponents with angular momenta up to $l = 3$, for a total of 68 basis functions listed in Table I that reproduces the hydrogen atom ionization rates of large basis. Both of these basis sets yield accurate energies for hydrogen atom. For H_2^+, HCO^+, and HCl^+, the absorbing basis was added to a standard aug-cc-pVTZ basis.[44,45] In this case, the absorbing basis could be reduced even further to 31 functions, as indicated by the asterisks in Table I. For sake of simplicity in the following discussion, we call these basis sets the large, medium, and small absorbing basis sets.

The ionization rates of hydrogen atom were computed with *Mathematica 9*.[46] Because of the size of the absorbing basis sets and the placement of the CAP, there is a small residual absorption rate for ground state field-free hydrogen atom, 10^{-7} $E_h/\hbar$ (inverse atomic unit of time), that is several orders of magnitude smaller than the ionization rate in fields of 0.03 − 0.10 $E_h/(ea_0)$. The ionization rates computed with Gaussian and the Fortran code for TDCIS have been verified by comparing with the Mathematica results. Calculations on H_2^+, HCO^+, and HCl^+ used the standard Dunning aug-cc-pVTZ basis set[44,45] to ensure correct energetics. The absorbing basis set was placed on the two atoms involved in the bond dissociation. Because this could result in serious linear dependency problems in the basis set expansion, simulations were also carried out with the absorbing basis placed only on a ghost atom in the middle of the dissociating bond. The CAP also has a contribution from the ghost atom, which is chosen to have the same radius as a hydrogen atom.

III. NUMERICAL RESULTS

A. Ionization rates for H atom

Complex absorbing potentials were used to calculate the ionization of hydrogen atom for a series of electric fields increasing from 0.03 to 0.10 $E_h/(ea_0)$. In order to simulate the ionization in a strong static field with the time-dependent methodology, the field is turned on slowly until it reaches a maximal value and then stays constant. Under such a quasi-static field, the norm of the wavefunction decays exponentially from which we obtain the rate. We compare our findings with the work from accurate, grid based simulations.[7,8]

Using the medium absorbing basis shown in Table I, the ground state energy is −0.49901 and the first excited state is −0.12489 E_h, compared to the exact values of −0.5 and −0.125 E_h. The polarizability is 4.52011 a_0^3 calculated from sum-over-states formula, which is just slightly higher than the exact value of 4.5 a_0^3 for the hydrogen atom.

The adiabatic dynamics for fields of $E_{max} = 0.04, 0.06,$ 0.08 $E_h/(ea_0)$ are shown in Fig. 2. The electric field is gradually ramped to its maximum value (Fig. 2(a)). The electron density follows the applied field adiabatically, as can be seen from the progression of the dipole moment (Fig. 2(b)). Just before the field reached its maximal value, the tail of the electron density reaches the CAP, and thereafter the norm decays exponentially (Fig. 2(c)). Rather than a wavepacket driven towards the CAP, there is a steady state decaying with time (Fig. 3). For $E_{max} = 0.06$ $E_h/(ea_0)$, the norm of the wavefunction decreased by about 20% in about 45 fs. From the exponential loss of the norm during the constant field, a rate easily

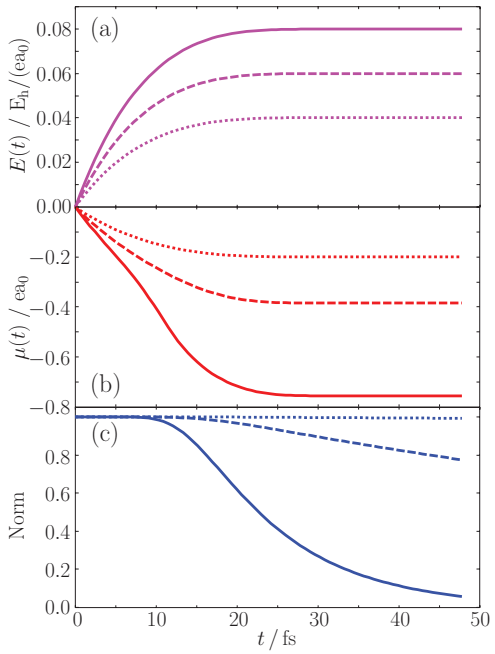

FIG. 2. Ionization of hydrogen atom with fields of 0.04 $E_h/(ea_0)$ (dotted), 0.06 $E_h/(ea_0)$ (dashed), 0.08 $E_h/(ea_0)$ (solid): (a) the field amplitude of the quasi-static pulse, (b) time-dependent dipole moment, and (c) exponential decay of the wavefunction norm as a result of the CAP.

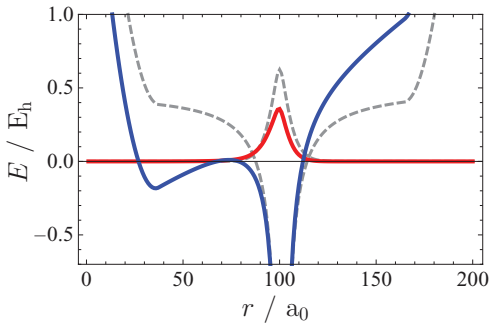

FIG. 3. One-dimensional cut through the hydrogen atom. The Coulomb potential plus the absolute value of the CAP and electron density are shown for two time steps: in dashed for $t = 0$ and solid for $t = 45$ fs at a field strength of 0.06 $E_h/(ea_0)$ (see Fig. 2).

can be calculated. This rate is interpreted as the ionization rate.

Depending on the field strength, ionization can take place by either tunneling through the Coulomb barrier, or above threshold, when the barrier is suppressed completely by the field. The two regimes can be distinguished by the Keldish parameter, $\gamma = \sqrt{I_p/2U_p}$, where I_p is the ionization potential and $U_p = |E_0|^2/4\omega^2$ is the ponderomotive energy. For $\gamma < 1$ ionization takes place by tunneling through the barrier, whereas for $\gamma > 1$, above threshold ionization takes place. For hydrogen atom in a laser field with a frequency of 0.057 $E_h/\hbar$, ionization changes from tunneling to above threshold as the field strength increases above 0.06 $E_h/(ea_0)$.

Figure 4 shows the ionization rates as a function of the maximum field strength, E_{max}. The simulated field strengths cover the regimes of tunnel ionization and above threshold ionization. Simulations are shown for the medium and large absorbing basis. Also plotted are the reference values obtained from large, grid based calculations.[7,8] Our absolute rates are in good agreement with the reference values for field strength greater than 0.04 $E_h/(ea_0)$. For better agreement at lower field strengths, the CAP would have to be placed further from the nucleus and the basis set would have to contain

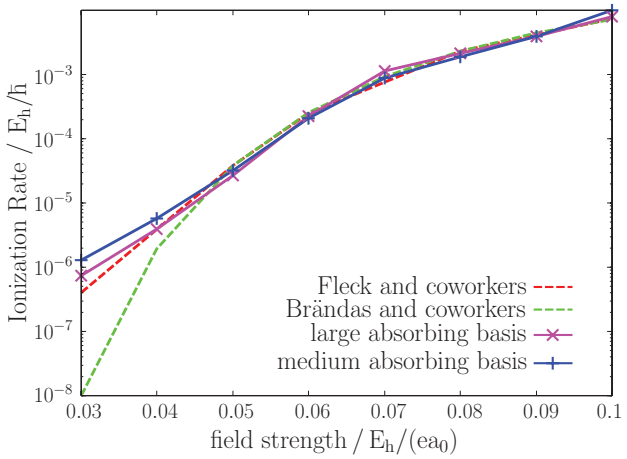

FIG. 4. Ionization rates for hydrogen atom on a logarithmic scale for the medium and large absorbing basis sets compared to accurate, grid based calculations from Refs. 7 and 8.

additional diffuse functions. The good agreement between the medium and large absorbing basis sets was obtained by selectively deleting the basis functions from the large absorbing basis that did not contribute significantly to the rate.

B. Charge resonance enhanced ionization in H_2^+

Intense field molecular ionizations show strong enhancements in the rate for certain longer bond lengths.[9,10,34,47–50] For H_2^+ and H_2, it has been shown that charge resonance transitions and localization of the electronic wavefunction are responsible for this Charge-Resonance Enhanced Ionization (CREI) at critical internuclear distances.[47,48]

Several numerical simulations have been carried out for the ionization of H_2^+ as a function of bond length. Bandrauk and co-workers have performed accurate 3D grid based simulations of the ionization probability for laser fields aligned with the bond at frequencies of 0.057 $E_h/\hbar$ (800 nm) and 0.043 $E_h/\hbar$ (1064 nm).[9,49] Hansen and co-workers have studied H_2 ionization as a function of bond length and orientation with accurate 3D simulations using a combination radial grids and spherical harmonics.[10] Uhlmann *et al.* have calculated the bond length dependence of H_2 ionization using a basis set expansion approach and an absorbing potential.[34] Recently, Becker and co-workers have used 2D grid based calculations to simulate ionization, vibrational excitation, and dissociation of H_2^+ as a function of the laser pulse intensity, wavelength, and duration.[13]

To compare with the H_2^+ results of Bandrauk and co-workers,[9,49] we carried out a series of TDCIS calculations with CAP to model the change in the ionization rate with increasing internuclear distances. The linearly polarized laser pulses had carrier frequencies of 0.057 $E_h/\hbar$ and 0.043 $E_h/\hbar$ and were aligned parallel and perpendicular to the molecular axis. The pulses had a cosine square shape and consisted of 5 cycles with maximal field strength of 0.0534 $E_h/(ea_0)$, corresponding to an intensity of 1.00×10^{14} W/cm^2. The standard Dunning aug-cc-pVTZ basis set[44,45] was used on the hydrogens and the medium absorbing basis was placed on a ghost atom at the bond midpoint. The CAP used $r_a = 9.524$ a_0 for the hydrogens and the ghost atom. The ionization rate was calculated from the norm loss divided by the pulse duration:

$$\Gamma_{ion} = (1 - N(t_{end}))/2\sigma, \tag{8}$$

where $N(t_{end})$ is the norm of the wavefunction at the end of the pulse and 2σ is the full pulse duration, 13.34 fs for $\hbar\omega = 0.057$ $E_h$and 17.75 fs for $\hbar\omega = 0.043$ E_h, respectively.

Figure 5 shows the ionization rates as a function of the nuclear separation R. For perpendicular laser polarization (green, short dash), the ionization rate increases a little around $R = 6$ a_0 and stays almost constant after $R = 9$ a_0. This rise at $R = 6$ a_0 is governed by atomic-like transitions since the Coulomb potential for the perpendicular polarization is a single well. For polarizations parallel to the molecular axis, the ionization is greatly enhanced and a distinct peak structure is visible. The position of the peaks compares very well with the results of Bandrauk and co-workers[49] reproduced in Fig. 6. Because of the difference in the pulse shape, our

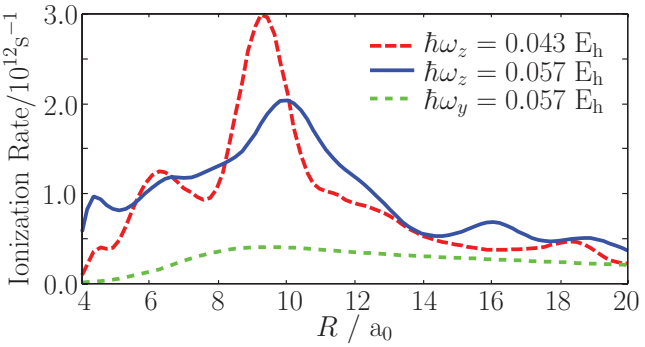

FIG. 5. Ionization rates for H_2^+ as function of internuclear distance modelled with TDCIS and CAP. The aug-cc-pVTZ was used for the H atoms and the medium absorbing basis was placed on a ghost atom at the mid-point of the bond. A 5 cycle cosine squared pulse with frequencies of 0.057 $E_h/\hbar$ (800 nm) and 0.043 $E_h/\hbar$ (1064 nm) and a maximum intensity of 1.00×10^{14} W/cm^2 was aligned parallel (ω_z) and perpendicular (ω_y) to the molecular axis.

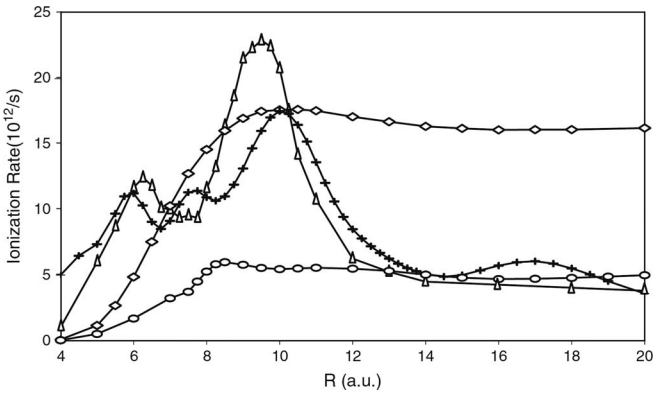

FIG. 6. Ionization rates for H_2^+ vs R for (i) $I = 10^{14}$ W/cm^2, linear polarization parallel to R (z-axis): (a) (plus): $\lambda = 800$ nm; (b) (open triangles): $\lambda = 1064$ nm, and (c) (open circle): $\lambda = 800$ nm, perpendicular to R and (ii) $I = 2 \times 10^{14}$ W/cm^2, circular polarization in x-y plane, $\lambda = 800$ nm: (open diamond). From A. D. Bandrauk and F. Legare, *Progress in Ultrafast Intense Laser Science VIII*, Copyright 2012 by Springer-Verlag. Reprinted by permission of Springer-Verlag.

calculated ionization rates are about an order of magnitude smaller than the ones calculated by Bandrauk.

The ionization rate as a function of the internuclear distance has been discussed extensively by Bandrauk.[49] The peak near $R = 6$ a$_0$ corresponds a one photon resonance for the $\sigma_g \rightarrow \sigma_u$ transition. The pronounced peak near $R = 9$ a$_0$ is the result of CREI. A few smaller peaks present in Fig. 5 but absent in Fig. 6 are probably basis set related. When the basis set is increased from aug-cc-pVTZ to aug-cc-pVQZ or when the large absorbing basis, limited to $l = 0$–3, is placed on the ghost atom (for a total of 318 basis functions for the system),the relative heights and positions of some of the small bands change only a little.

C. Enhanced ionization in HCl^+ and HCO^+

The strength of the present approach is that it can be applied to many-electron polyatomic systems. As an initial test, we have examined the ionization of HCl^+ and HCO^+ as a function of bond length. Ground state dissociation of both systems can be described at the Hartree-Fock level and the lowest excited states can be treated by CIS. The laser pulse parameters were the same as for H_2^+ (linearly polarized 5 cycle cosine squared pulse aligned with the bond axis with frequencies of 0.057 $E_h/\hbar$ (800 nm) and 0.043 $E_h/\hbar$ (1064 nm) and a maximal field strength of 0.0534 $E_h/(ea_0)$, corresponding to an intensity of 1.00×10^{14} W/cm^2). The aug-cc-pVTZ basis set was used for the atoms, and the medium absorbing basis was placed on a ghost atom in the middle of the dissociating bond or on the two atoms of the dissociating bond, or the small absorbing basis was placed on all atoms. For the CAP, r_a was set to 3.5 times the van der Waals radius (9.544, 13.053, 12.735, 11.575 a$_0$ for H, Cl, C, O, respectively).

Figures 7 and 9 show the excitation energies and ionization probabilities for HCl^+ and HCO^+ as a function of the bond distance. For HCO^+ the CO bond length was fixed at 2.037a$_0$ (1.078 Å). The TDCIS calculations for HCl^+ and HCO^+ with the aug-cc-pVTZ basis involve 452 and 541 states without the absorbing basis, and approximately 920 and 880 states with the medium absorbing basis on a ghost atom in the middle of the bond. With placing the medium absorbing basis on the two atoms of the dissociating bond, CIS leads to about 1350 and 1170 states, and approximately 780 and 870 states with the small absorbing basis on all atoms.

Figure 7(b) shows the results for simulations of HCl^+ with $\hbar\omega = 0.057$ E$_h$. When only the aug-cc-pVTZ basis is used, some enhancement of the ionization rate is seen around

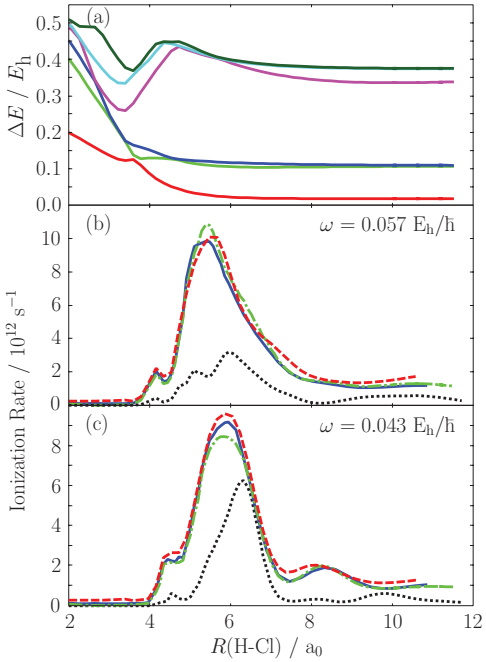

FIG. 7. Excitation energies and ionization rates as a function of bond length for HCl^+ in a 5 cycle cosine squared pulse aligned with the bond axis and with a maximal field strength of 0.0534 $E_h/(ea_0)$. (a) Lowest 6 excited states for field free HCl^+ calculated at the CIS/aug-cc-pVTZ level of theory with the medium absorbing basis on a ghost atom at the bond midpoint, (b) ionization rates for a frequency of 0.057 $E_h/\hbar$ (800 nm), (c) ionization rates for a frequency of 0.043 $E_h/\hbar$ (1064 nm). Dotted black line – aug-cc-pVTZ basis, dashed-dotted green line – aug-cc-pVTZ plus medium absorbing basis at the bond midpoint, solid blue line – aug-cc-pVTZ plus medium absorbing basis on H and C, dashed red line – small absorbing basis on H and Cl.

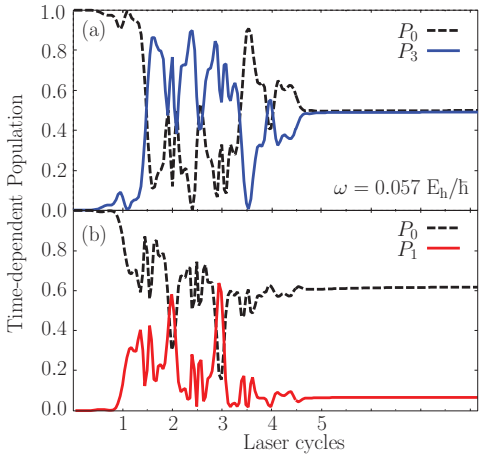

FIG. 8. Time-dependent populations for the ground state and excited states of (a) HCl^+ and (b) HCO^+ at bond length of $R = 5.5a_0$ (2.9 Å) in a 5 cycle cosine squared pulse with the frequency of 0.057 $E_h/\hbar$ (800 nm) and with a maximal field strength of 0.0534 $E_h/(ea_0)$.

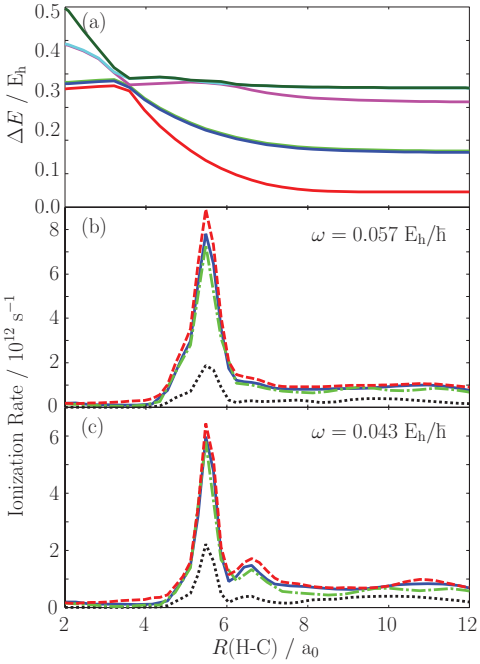

FIG. 9. Excitation energies and ionization rates as a function of bond length for HCO^+ in a 5 cycle cosine squared pulse aligned with the bond axis and with a maximal field strength of 0.0534 $E_h/(ea_0)$. (a) Lowest 6 excited states for field free HCO^+ calculated at the CIS/aug-cc-pVTZ level of theory (with the absorbing basis), (b) ionization rates for a frequency of 0.057 $E_h/\hbar$ (800 nm), (c) ionization rates for a frequency of 0.043 $E_h/\hbar$ (1064 nm). Dotted black line – aug-cc-pVTZ basis, dashed-dotted green line – aug-cc-pVTZ plus medium absorbing basis at the bond midpoint, solid blue line – aug-cc-pVTZ plus medium absorbing basis on H and C, dashed red line – small absorbing basis on H, C, and O.

$R = 6$ a_0 and 10 a_0. When the absorbing basis is included, the ionization rate near $R = 6$ a_0 increases by almost a factor of three. For $\hbar\omega = 0.043$ E_h, Fig. 7(c), the peak is high even without the absorbing basis. In both cases, placing the absorbing basis on a ghost atom in the middle of the bond has about the same effect as putting it on the two atoms. Populations of the strongly coupled states during the pulse are shown in Fig. 8. For bond lengths greater than about $5a_0$, the field-free ground state of HCl^+ can be described as triplet Cl^+ antiferromagnetically coupled to doublet hydrogen atom. The third excited state is the lowest state with a transition dipole along the bond axis and is the only state that gains significant population during the pulse. The transition dipole peaks near $5a_0$ and diminishes rapidly to zero around $11a_0$. The transition from the ground state to the third excited state involves the transfer of an electron from the hydrogen 1*s* orbital to the chlorine $3p_\sigma$ orbital, yielding neutral Cl and H^+. This transition couples strongly to a laser field aligned with the bond, as can be seen in Fig. 8(a). The result is enhanced ionization in a manner analogous to CREI in H_2^+.

The corresponding results for HCO^+ are reported in Figs. 9 and 8(b). Enhanced ionization is seen between 4 and 7 a_0. At $\hbar\omega = 0.057$ E_h, there is a large peak at 5.5 a_0. This large peak becomes narrower for $\hbar\omega = 0.043$ E_h, and a second, smaller peak appears around 6.6 a_0. In all cases, placing the medium absorbing basis at the bond mid-point or on the H and C atoms or using the small absorbing basis on all the atoms has about the same effect on the ionization rate. Increasing the atomic basis to aug-cc-pVQZ results in very little change (not shown). This suggests that aug-cc-pVTZ with the medium absorbing basis at the bond mid-point or the small absorbing basis on all atoms is sufficient for modeling the enhancement of ionization as the bond is stretched. For moderate elongation of the CH bond, the highest occupied orbital is σ_{CH} and the lowest unoccupied orbital is σ^*_{CH}. As the bond is stretched further, the highest occupied orbital becomes a σ lone pair on carbon and the lowest unoccupied orbital becomes a 1*s* orbital on hydrogen. The ground state can be described as H^+-CO and the lowest excited state looks like H atom and CO^+. The transition dipole for the ground to first excited state reaches a broad maximum near $4a_0$ and decays toward zero by $11a_0$. Figure 8(b) shows a large population of the lowest electronic states that are coupled during the pulse. Later in the pulse there is also significant population of the $H^* + CO^+$ states which involve excitation from the CO π orbitals to the hydrogen $2p$ orbitals. These processes indicate that a CREI-like mechanism contributes to the enhanced ionization in HCO^+ as the bond is elongated.

IV. CONCLUSION

We have shown that it is possible to model ionization rates by solving the time-dependent Schrödinger equation using atom-centered basis sets and an absorbing potential. We found very good agreements for the calculation of absolute ionization rates for the H atom. Our approach shows that we can cover the tunnel regime as well as above barrier ionization. For H_2^+ large ionization rates due to CREI are well represented. Whereas the accurate grid based methods are suitable for one electron systems, the present method can be applied to many electron polyatomic systems. Our calculations on HCl^+ and HCO^+ show that CREI can also be seen in larger systems.

ACKNOWLEDGMENTS

This work was supported by a grand from the National Science Foundation (CHE1212281). We thank Wayne State University's computing grid for computer time.

[1]M. Hentschel, R. Kienberger, Ch. Spielmann, G. A. Reider, N. Milosevic, T. Brabec, P. Corkum, U. Heinzmann, M. Drescher, and F. Krausz, Nature (London) **414**, 509 (2001).
[2]M. Drescher, M. Hentschel, R. Kienberger, M. Uiberacker, V. Yakovlev, A. Scrinzi, Th. Westerwalbesloh, U. Kleineberg, U. Heinzmann, and F. Krausz, Nature (London) **419**, 803 (2002).
[3]H. Niikura, D. M. Villeneuve, and P. B. Corkum, Phys. Rev. Lett. **94**, 083003 (2005).
[4]E. Goulielmakis, M. Schultze, M. Hofstetter, V. S. Yakovlev, J. Gagnon, M. Uiberacker, A. L. Aquila, E. M. Gullikson, D. T. Attwood, R. Kienberger *et al.*, Science **320**, 1614 (2008).
[5]X. Liu, H. Rottke, E. Eremina, W. Sandner, E. Goulielmakis, K. O. Keeffe, M. Lezius, F. Krausz, F. Lindner, M. G. Schätzel *et al.*, Phys. Rev. Lett. **93**, 263001 (2004).
[6]J. Itatani, J. Levesque, D. Zeidler, H. Niikura, H. Pépin, J. C. Kieffer, P. B. Corkum, and D. M. Villeneuve, Nature (London) **432**, 867 (2004).
[7]M. R. Hermann and J. A. Fleck, Jr., Phys. Rev. A **38**, 6000 (1988).
[8]M. Hehenberger, H. V. McIntosh, and E. Brändas, Phys. Rev. A **10**, 1494 (1974).
[9]A. D. Bandrauk and H. Z. Lu, Phys. Rev. A **62**, 053406 (2000).
[10]T. K. Kjeldsen, L. B. Madsen, and J. P. Hansen, Phys. Rev. A **74**, 035402 (2006).
[11]K. Harumiya, H. Kono, Y. Fujimura, I. Kawata, and A. D. Bandrauk, Phys. Rev. A **66**, 043403 (2002).
[12]E. Dehghanian, A. D. Bandrauk, and G. L. Kamta, Phys. Rev. A **81**, 061403 (2010).
[13]A. Picón, A. Jaroń-Becker, and A. Becker, Phys. Rev. Lett. **109**, 163002 (2012).
[14]K. C. Kulander, Phys. Rev. A **36**, 2726 (1987).
[15]E. Runge and E. K. U. Gross, Phys. Rev. Lett. **52**, 997 (1984).
[16]P. Krause, T. Klamroth, and P. Saalfrank, J. Chem. Phys. **123**, 074105 (2005).
[17]F. Remacle, R. Kienberger, F. Krausz, and R. D. Levine, Chem. Phys. **338**, 342 (2007).
[18]H. B. Schlegel, S. M. Smith, and X. Li, J. Chem. Phys. **126**, 244110 (2007).
[19]L. Greenman, P. J. Ho, E. Karmarchik, D. A. Mazzoni, and R. Santra, Phys. Rev. A **82**, 023406 (2010).
[20]C. Huber and T. Klamroth, J. Chem. Phys. **134**, 054113 (2011).
[21]S. Kvaal, J. Chem. Phys. **136**, 194109 (2012).
[22]F. Remacle, M. Nest, and R. D. Levine, Phys. Rev. Lett. **99**, 183902 (2007).
[23]M. Nest, T. Klamroth, and P. Saalfrank, Z. Phys. Chem. **224**, 569 (2010).
[24]H. Miyagi and L. B. Madsen, Phys. Rev. A **87**, 062511 (2013).
[25]T. Sato and K. L. Ishikawa, Phys. Rev. A **88**, 023402 (2013).
[26]P. Krause, T. Klamroth, and P. Saalfrank, J. Chem. Phys. **127**, 034107 (2007).
[27]J. A. Sonk, M. Caricato, and H. B. Schlegel, J. Phys. Chem. A **115**, 4678 (2011).
[28]P. Krause, T. Klamroth, and P. Saalfrank, J. Chem. Phys. **128**, 234307 (2008).
[29]I. Barth, J. Manz, Y. Shigeta, and K. Yagi, J. Am. Chem. Soc. **128**, 7043 (2006).
[30]T. Klamroth, J. Chem. Phys. **124**, 144310 (2006).
[31]J. Breidbach and L. S. Cederbaum, J. Chem. Phys. **118**, 3983 (2003).
[32]J. Breidbach and L. S. Cederbaum, J. Chem. Phys. **126**, 034101 (2007).
[33]G. Periyasamy, R. D. Levine, and F. Remacle, Chem. Phys. **366**, 129 (2009).
[34]M. Uhlmann, T. Kunert, and R. Schmidt, J. Phys. B: At. Mol. Opt. Phys. **39**, 2989 (2006).
[35]S. Klinkusch, P. Saalfrank, and T. Klamroth, J. Chem. Phys. **131**, 114304 (2009).
[36]E. Luppi and M. Head-Gordon, J. Chem. Phys. **139**, 164121 (2013).
[37]J. B. Foresman, M. Head-Gordon, J. A. Pople, and M. J. Frisch, J. Phys. Chem. **96**, 135 (1992).
[38]M. J. Frisch, G. W. Trucks, H. B. Schlegel *et al.*, Gaussian Development Version, Revision H.20+, Gaussian, Inc., Wallingford, CT, 2010.
[39]U. V. Riss and H.-D. Meyer, J. Chem. Phys. **105**, 1409 (1996).
[40]D. Kosloff and R. Kosloff, J. Comput. Phys. **63**, 363 (1986).
[41]J. Tomasi, B. Mennucci, and R. Cammi, Chem. Rev. **105**, 2999 (2005).
[42]A. D. Becke, J. Chem. Phys. **88**, 2547 (1988).
[43]V. I. Lebedev and A. L. Skorokhodov, Dokl. Akad. Nauk **324**, 519–524 (1992).
[44]T. H. Dunning, Jr., J. Chem. Phys. **90**, 1007 (1989).
[45]A. K. Wilson, T. van Mourik, and T. H. Dunning, Jr., J. Mol. Struct.: THEOCHEM **388**, 339 (1996).
[46]*Mathematica 9.0*, Wolram Reseach Inc., Champain, IL (2012).
[47]T. Seideman, M. Y. Ivanov, and P. B. Corkum, Phys. Rev. Lett. **75**, 2819 (1995).
[48]T. Zuo and A. D. Bandrauk, Phys. Rev. A **52**, R2511(R) (1995).
[49]A. D. Bandrauk and F. Légaré, *Enhanced Ionization of Molecules in Intense Laser Fields* (Springer, Berlin/Heidelberg, 2012), Vol. 8, Chap. 2, pp. 29–46.
[50]E. Dehghanian, A. D. Bandrauk, and G. Lagmago Kamta, J. Chem. Phys. **139**, 084315 (2013).